arXiv:1407.1125v2 [cond-mat.supr-con] 14 Jan 2015

Topological *s*-wave pairing superconductivity with spatial inhomogeneity: Mid-gap-state appearance and robustness of superconductivity

Yuki Nagai, Yukihiro Ota, and Masahiko Machida

CCSE, Japan Atomic Energy Agency, 178-4-4, Wakashiba, Kashiwa, Chiba, 277-0871, Japan

We study the quasiparticle spectrum of 2D topological *s*-wave superconductors with the Zeeman magnetic field and the Rashba spin-orbit coupling in the presence of spatial inhomogeneity. Solving the real-space Bogoliubov-de Gennes equations, we focus on the excitations within the superconducting gap amplitude, i.e., the appearance of mid-gap states. Two kinds of potential functions, line-type (a chain of impurities) and point-type (a single impurity) ones are examined to take spatial inhomogeneity into account. The line setting shows a link of the mid-gap states with the gapless surface modes indicated by the bulk-boundary correspondence in topological superfluid. The point one shows that the quasiparticles with mid-gap energy are much easily excited by an impurity when the Zeeman magnetic field increases within the topological number to be unchanged. Thus, we obtain insights into the robustness of a topological superconductor against non-magnetic impurities. Moreover, we derive an effective theory applicable to high magnetic fields. The effective gap is the mixture of the chiral *p*-wave and *s*-wave characters. The former is predominant when the magnetic field increases. Therefore, we claim that a chiral *p*-wave character of the effective gap function creates the mid-gap states.

1. Introduction

One of the fundamental issues in superconductivity is to study impurity effects. A statement about the response to non-magnetic impurities, so-called Anderson's theorem plays a central role in this issue; no significant T_c reduction by non-magnetic impurities occurs in *s*-wave superconductivity.[1–5] In other words, the impurities produce no additional pole in the Green's function within energy scale characterized by superconducting gap amplitude. Thus, when the impurities lead to the decrease of T_c, the reduction can be related to poles inside gap energy, mid-gap states (MGSs).[6–11]

Studying topological superconductors[12–15] is an exciting research topic in condensed matter physics now. The bulk-boundary correspondence[16] in topological materials implies the presence of gapless (zero-energy) modes around defects, as well as on surfaces. The gapless modes around defects in topological superconductors are studied in detail.[17–19] However, the impurity effects, especially the decrease of T_c are not discussed fully, although both impurities and defects induce spatial inhomogeneity into bulk systems.

Nagai *et al.*[27] studied the non-magnetic impurity effects in a 2D topological superconductor with on-site *s*-wave pairing, using a self-consistent T-matrix approach. No considerable T_c decrease is found in a weak Zeeman magnetic field. However, the decrease via non-magnetic impurities is significant in a certain case. The reduction is more pronounced when the value of a topological number increases; a state with a non-zero even topological number significantly suffers from non-magnetic impurities, like an unconventional superconducting state. Since this topological number is related to the number of the gapless surface modes,[15] the authors infer from this result that the robustness of this topological *s*-wave pairing superconductor against non-magnetic impurities is related to the gapless surface modes. Therefore, it is worth asking how the MGSs induced by an impurity are related to the gapless surface modes, and how the unconventional feature appears in *s*-wave pairing.

In this article, we study the quasiparticle excitations in a topological superconductor with spatial inhomogeneity. We focus on a 2D topological superconducting model,[14,15] with on-site *s*-wave pairing, the Rashba spin-orbit coupling, and the Zeeman magnetic field. The model for the inhomogeneity is made by adding a local potential term to the uniform system. We examine two kinds of the setting, line-type and point-type potentials. The former is regarded as a straight chain of non-magnetic impurities, while the latter is a single one.

Changing the Zeeman magnetic field and the potential height, the quasiparticle spectrum is calculated numerically. Throughout this article, we focus on a topological phase in which the topological number is 1. We find that the both potential models induce the MGSs when the system lies in the topological phase. The resultant states are locally bound in the vicinity of the potential.

We obtain insights into the robustness of the topological superconducting state against non-magnetic impurity, depending on potential geometry. The line setting definitely shows a continuous connection of the MGSs into the zero-energy bound states, changing the potential into a hard-wall one. Thus, the MGSs in the present model have a link with the gapless surface modes indicated by the bulk-boundary correspondence, in a certain setup. The point setting indicates that the quasiparticles with mid-gap energy are much easily excited by impurities when the Zeeman magnetic field increases within the topological phase. We find that this result is consistent with the prediction on the decrease of T_c in Ref. 27.

To understand the numerical results, we discuss why the potential terms produce the MGSs. From the results in the point setting, we consider that an effective theory to describe a high-magnetic-field case is useful for the arguments. Thus,

we derive an effective gap function in the system without the potential term, by perturbation about the inverse of the magnetic-field strength. We find that the effective gap is the mixture of the chiral *p*-wave and *s*-wave components. The former becomes primary in the effective gap when the magnetic field increases. Hence, we claim that a chiral *p*-wave feature in the effective gap function creates the MGSs.

The article is organized as follows. In Sec. 2, we explain our motivation, mainly focusing on the previous theoretical studies about the non-magnetic impurity effects in the *s*-wave superconductivity. In Sec. 3, we explain a model of the 2D topological *s*-wave superconductors. The quasiparticle spectrum for line-type potential is shown in Sec. 4.1, and subsequently the results for the point-type one are shown in Sec. 4.2. In Sec. 5, we shows the discussions to understand better the numerical results. Specifically, we derive an effective gap function with both the chiral *p*-wave and *s*-wave characters in Sec. 5.3. In Sec. 6, the summary is shown.

2. Motivation and aim

The main issue in this article has a link with the impurity effects in superconductivity. To clarify our motivation, we summarize several theoretical results about superconducting alloys. Then, we show the aim in this article, focusing on our previous results about non-magnetic impurity effects.[27]

2.1 Anderson's theorem

A well-known result in the impurity effects is Anderson's theorem.[1] The critical temperature in *s*-wave superconductors does not significantly decrease by non-magnetic impurities. The idea is to focus on Kramers-degenerate electrons. If a metal has the time-reversal symmetry, the instability leading to superconductivity comes from the time-reversed pairs of electrons on the Fermi surface. Then, the perturbation not splitting the Kramers degeneracy has no effect on T_c.

It is an important issue in superconductivity to ask how T_c decreases in the presence of impurities when the conditions in the above argument are changed. Several ways of changing the conditions are available. One way is to change the superconducting character, keeping the time-reversal property of the normal electrons. Another way is to violate the time-reversal symmetry, with *s*-wave pairing. Considering spin-orbit couplings can also lead to the change of the conditions, since their absence is implicitly assumed in the typical arguments of Anderson's theorem.[3]

2.2 Mid-gap-state appearance in various settings

Since Anderson's theorem includes an argument of T_c, the quantitative discussion is needed for studying the validity in various physical settings. Studying the response to magnetic impurities gives us a clue for this issue. Magnetic impurities lead to the decrease of T_c in *s*-wave superconductors.[3,5] This is associated with the formation of the bound states around the impurities, with mid-gap energy $E \in (-\Delta, \Delta)$, where Δ is the superconducting gap amplitude. The mid-gap-state appearance corresponds to the occurrence of additional poles in the Green's functions. The modification of the anomalous Green's functions can change T_c.

We summarize the theoretical results on the impurity effects in the *s*-wave superconductivity, relevant to our issue.

2.2.1 Magnetic impurities

The presence of magnetic impurities leads to significant decrease of T_c.[3,5] This is related to the appearance of additional poles in the Green's functions, as pointed out above.

2.2.2 Zeeman magnetic field and non-magnetic impurities

Zeeman magnetic field breaks time reversal symmetry. One can expect that an *s*-wave superconducting state in the presence of the Zeeman magnetic field is not robust against non-magnetic impurities. The expectation is partially correct, but not always holds. We will argue this point below.

Ohashi[21] proposed a way of making a magnetic impurity in superfluid fermionic gases and showed the formation of bound states in an *s*-wave state. The keys of creating a magnetic impurity are to make Zeeman field by the population imbalance between atomic components and to use so strong on-site pairing potential that the Hartree term is predominant. Thus, the interplay between a non-magnetic impurity and the Zeeman field leads to the mid-gap-state appearance, under strong on-site pairing potential. However, in a weak-coupling superconducting theory the Hartree term is negligible.

Using a weak-coupling approach, Sau and Demler[22] studied the formation of bound states by impurities in a semiconductor nanowire in the proximity to an *s*-wave superconductor, similar to our model; both the Zeeman field and the spin-orbit coupling are involved. They point out that no MGS bound to non-magnetic impurities is found when the magnetic field takes a non-zero value, but the spin-orbit coupling vanishes. The form of the Green's functions in the system without impurities supports this statement. One can find that when only the Zeeman magnetic field exists, the Green's functions are expressed by a block diagonal matrix with two sectors, each of which is composed of the ones in the Bardeen-Cooper-Schrieffer theory. The Zeeman magnetic field gives an energy shift in the Green's functions.[23] Thus, using the standard arguments that non-magnetic impurity do not induce the bound states in *s*-wave superconductors, the assertion is obtained.

The above arguments indicate that the non-magnetic impurity effects under the Zeeman magnetic field are not so simply understood by the magnetic-impurity effects. We remark that our target is a weak-coupling *s*-wave superconductor.

2.2.3 Spin-orbit couplings and non-magnetic impurities

Studying specific models with spin-orbit couplings shows a similar statement to Anderson's theorem. Non-magnetic disorder has no effect on the critical temperature in a non-centrosymmetric superconductor with *s*-wave pairing.[24] In the proximity-induced superconductivity in a semiconductor nanowire only with the Rashba spin-orbit coupling,[22] no additional pole in the Green's function appears by a non-magnetic impurity.

2.3 *Impurity effects and a topological number*

The presence of *both* the Rashba spin-orbit coupling and the Zeeman magnetic field lead to non-trivial response to non-magnetic impurities.[22,25,27] To see this point, we summarize our previous results[27] in a 2D *s*-wave topological superconductor. The detail of the model is explained in Sec. 3.

Nagai *et al.*[27] numerically calculated T_c in the presence of non-magnetic impurities, using a self-consistent T-matrix approach. When the system in the clean limit lies in a non-topological region (i.e., a low-magnetic-field region), no significant T_c reduction occurs by non-magnetic impurities. However, the decrease of T_c appears when taking a higher magnetic field. Moreover, the calculations of a topological invariant, Thouless-Kohmoto-Nightingale-Nijs (TKNN) number[26] indicate the presence of a correlation of the TKNN number with the T_c reduction; the reduction is more pronounced when the TKNN number increases. We remark that the proximity-induced superconductivity in a semiconductor nanowire[22] also shows the formation of a bound state around a non-magnetic impurity, increasing the Zeeman magnetic field with non-zero spin-orbit coupling.

2.4 *Settings in the present issue: Potential models*

The above results motivate us to examine how in our model the mid-gap-state appearance connects with a topological property of the system. We focus on the fact that in the clean-limit bulk system the TKNN number is related to the number of the gapless surface modes in the system with edges.[15] Thus, it is a meaningful issue to consider the relation of the mid-gap-state appearance with the gapless surface modes indicated by the bulk-boundary correspondence. Studying the production of bound states [with energy $E \in (-\Delta, \Delta)$] in potential models is suitable for this issue. Changing potential strength, one can examine the bound-state production by both a impurity (i.e., finite barrier) and a defect (i.e., infinitely-high barrier).

Now, we show the settings in this article. We focus on two kinds of potential models, line-type potential and point-type potential, as seen in Fig. 2. The line-type potential may deform into a rigid wall through increase of the strength. The setup is also regarded as a straight chain of impurities. Thus, we first study the line setting, to understand the mid-gap-state appearance in terms of the bulk-boundary correspondence. A line segment can be a point when one shortens the line length continuously. Therefore, our next task is to study the point-type potential, as a limit of the line setting. The point setting is related to the calculations of T_c with a T-matrix approach when the impurity concentration is quite low.

3. Model

The system is described by a tight-binding model on an $N_x \times N_y$ square lattice, with on-site *s*-wave pairing and the Rashba spin-orbit coupling. Moreover, the Zeeman magnetic field is applied along the direction perpendicular to the *xy*-plane. The mean-field Hamiltonian is

$$\begin{aligned}\hat{H} &= -t\sum_{<j,j'>}\sum_{\sigma}\hat{c}^{\dagger}_{j,\sigma}\hat{c}_{j',\sigma} - \mu\sum_{j}\sum_{\sigma}\hat{c}^{\dagger}_{j,\sigma}\hat{c}_{j,\sigma} \\ &\quad -\frac{\alpha}{2}\sum_{j}[(\hat{c}^{\dagger}_{j-e_x,\downarrow}\hat{c}_{j,\uparrow} - \hat{c}^{\dagger}_{j+e_x,\downarrow}\hat{c}_{j,\uparrow}) \\ &\quad +i(\hat{c}^{\dagger}_{j-e_y,\downarrow}\hat{c}_{j,\uparrow} - \hat{c}^{\dagger}_{j+e_y,\downarrow}\hat{c}_{j,\uparrow}) + \text{h.c.}] \\ &\quad -h\sum_{j}(\hat{c}^{\dagger}_{j,\uparrow}\hat{c}_{j,\uparrow} - \hat{c}^{\dagger}_{j,\uparrow}\hat{c}_{j,\uparrow}) \\ &\quad +\sum_{j}(\Delta\hat{c}^{\dagger}_{j,\uparrow}\hat{c}^{\dagger}_{j,\downarrow} + \text{h.c.}) + \sum_{j}\sum_{\sigma}V_j\hat{c}^{\dagger}_{j,\sigma}\hat{c}_{j,\sigma}, \quad (1)\end{aligned}$$

with the nearest neighbor hopping matrix element $t\,(>0)$, the chemical potential μ, the spin-orbit coupling constant $\alpha\,(>0)$, the magnitude of the Zeeman magnetic field h, and the superconducting gap Δ. The lattice constant is normalized by 1. The annihilation and creation operators of electrons with spin $\sigma\,(=\uparrow, \downarrow)$ are, respectively, $\hat{c}_{j,\sigma}$ and $\hat{c}^{\dagger}_{j,\sigma}$ on site $j = (j_x, j_y)$. In the third term, i.e., Rashba spin-orbit coupling, the symbol e_x means the unit vector along x-axis: $e_x = (1, 0)$. Similarly, e_y is the unit vector along y-axis. The last term is the potential term. We focus on two kinds of the potential functions; (i) line-type potential ($V_j = V^{(\mathrm{L})}_j$) and (ii) point-type potential ($V_j = V^{(\mathrm{P})}_j$), where

$$V^{(\mathrm{L})}_j = V\delta_{j_x,N_x/2}, \quad (2)$$

$$V^{(\mathrm{P})}_j = V\delta_{j_x,N_x/2}\,\delta_{j_y,N_y/2}. \quad (3)$$

The potential height V is positive (repulsive potential). We will use the Fourier-transformed model along y-axis, for case (i). Tight-binding Hamiltonian (1) is equivalent to a 2D topological superconducting model in ultra-cold atomic gases,[14,15] if the potential term is absent. Our model also describes a proximity-induced superconducting system on the interface between semiconductors and superconductors. In the junction systems, the potential term can be implemented by controlling the chemical potential via local gate voltage.[20]

Let us concisely summarize the topological properties of our system in clean limit ($V_j = 0$ for any j). The spatial uniformity allows us to write down the tight-binding Hamiltonian in momentum space. The electron annihilation and creation operators are, respectively, $\hat{c}_{\boldsymbol{k},\sigma}$ and $\hat{c}^{\dagger}_{\boldsymbol{k},\sigma}$. They are bound as the 4-component vectors, $\hat{\Psi}_{\boldsymbol{k}} = {}^{\mathrm{t}}(\hat{c}_{\boldsymbol{k},\uparrow}, \hat{c}^{\dagger}_{-\boldsymbol{k},\uparrow}, \hat{c}_{\boldsymbol{k},\downarrow}, \hat{c}^{\dagger}_{-\boldsymbol{k},\downarrow})$ and $\hat{\Psi}^{\dagger}_{\boldsymbol{k}} = (\hat{c}^{\dagger}_{\boldsymbol{k},\uparrow}, \hat{c}_{-\boldsymbol{k},\uparrow}, \hat{c}^{\dagger}_{\boldsymbol{k},\downarrow}, \hat{c}_{-\boldsymbol{k},\downarrow})$. We find that $\hat{H}|_{V=0} = (1/2)\sum_{\boldsymbol{k}}\hat{\Psi}^{\dagger}_{\boldsymbol{k}}\mathcal{H}_{\boldsymbol{k}}\hat{\Psi}_{\boldsymbol{k}}$, with the Bogoliubov-de Gennes (BdG) Hamiltonian,

$$\begin{aligned}\mathcal{H}_{\boldsymbol{k}} &= \frac{s^0+s^3}{2}\otimes(\varepsilon_{\boldsymbol{k}}-h)\tau^3 + \frac{s^0-s^3}{2}\otimes(\varepsilon_{\boldsymbol{k}}+h)\tau^3 \\ &\quad +s^1\otimes\alpha\ell_{1,\boldsymbol{k}}\tau^0 + s^2\otimes\alpha\ell_{2,\boldsymbol{k}}\tau^3 \\ &\quad +s^2\otimes(i\Delta\tau^+ + \text{h.c.}), \quad (4)\end{aligned}$$

where $\varepsilon_{\boldsymbol{k}} = -\mu - 2t(\cos k_x + \cos k_y)$, $\ell_{1,\boldsymbol{k}} = \sin k_y$, and $\ell_{2,\boldsymbol{k}} = -\sin k_x$. The ith component of the 2×2 Pauli matrices ($i = 1, 2, 3$) is written by s^i for spin. Similarly, the Pauli matrices for the Nambu space are written by τ^i. The 2×2 identity matrices for spin and the Nambu space are, respectively, s^0 and τ^0. The ladder operators in the Nambu space are defined by $\tau^{\pm} = (1/2)(\tau^1 \pm i\tau^2)$. The diagonalization of Eq. (4)

leads to the bulk spectrum

$$E(\boldsymbol{k}) = \sqrt{\varepsilon_{\boldsymbol{k}}^2 + \alpha^2|\boldsymbol{\ell}_{\boldsymbol{k}}|^2 + h^2 + |\Delta|^2 \pm 2\xi_{\boldsymbol{k}}}, \tag{5}$$

with $\boldsymbol{\ell}_{\boldsymbol{k}} = (\ell_{1,\boldsymbol{k}}, \ell_{2,\boldsymbol{k}})$ and $\xi_{\boldsymbol{k}} = \sqrt{\varepsilon_{\boldsymbol{k}}^2\alpha^2|\boldsymbol{\ell}_{\boldsymbol{k}}|^2 + (\varepsilon_{\boldsymbol{k}}^2 + |\Delta|^2)h^2}$. The topological phase transition occurs when the energy gap of bulk spectrum (5) closes at specific points in the Brillouin zone.[15] According to Table I in Ref. 15, the topological property of the superconducting state for $\mu > 2t$ and $h < 3t$ changes from a trivial phase to a non-trivial one, when h is greater than a critical value,

$$h > \sqrt{(4t-\mu)^2 + \Delta^2}. \tag{6}$$

4. Results

We numerically diagonalize tight-binding Hamiltonian (1), to examine the quasiparticle excitations in this system. The pair potential is $\Delta = 0.35t$ and the chemical potential is $\mu = 3.5t$, throughout this article. We accurately evaluate the eigenvalues and the eigenstates within $(-\Delta, \Delta)$, with a method by Sakurai and Sugiura.[28] The authors in Ref. 28 propose a practical way of solving a generalized eigenvalue problem, with a restricted eigenvalue domain. This approach leads to a numerical construction of a small-size effective Hamiltonian, keeping the essential properties of the original large-size Hamiltonian. The central idea is an efficient calculation of the projector onto an aimed energy domain. The contour integral for the projector on complex plain is approximated by numerical quadrature. The application to different superconducting issues and the detail implementation way are shown in Ref. 29.

4.1 Line-type potential

We concentrate on line-type potential (2). The set up is shown in Fig. 1(a). The translational symmetry along y-axis leads to a k_y-resolved Hamiltonian from Eq. (1). The number of the lattice size along x-axis is $N_x = 120$. We impose the periodic boundary condition along x-axis.

We study about the case of the Zeeman-magnetic-field strength to be $h = t$, for a while. We find that, from Eq. (6), a topological superconducting state occurs in the clean-limit bulk system. Figure 2 shows that the potential with $V = 100\,t$ induces the almost-zero-energy states. Since the system without the potential is in a topological phase, these zero-energy states are regarded as the gapless bound states on the surfaces of the potential wall. In other words, the line-type potential with $V = 100\,t$ can be regarded as a line defect, i.e., wall. This ultra-high potential barrier completely divides the system into the two subsystems, left and right parts; the left part is separated from the right part, by vacuum.

The result for the ultra-high-barrier line-type potential motivates us to study lower-barrier cases. Figure 3 shows the energy dispersions, with $V = 1\,t$, $5\,t$, and $10\,t$. We find that for $V = 5\,t$ and $10\,t$ the quasiparticle excitations occur, within the energy domain $(-\Delta, \Delta)$. Thus, the line-type potentials with either high or intermediate barriers induce the MGSs. Changing V means the continuous deformation of the energy

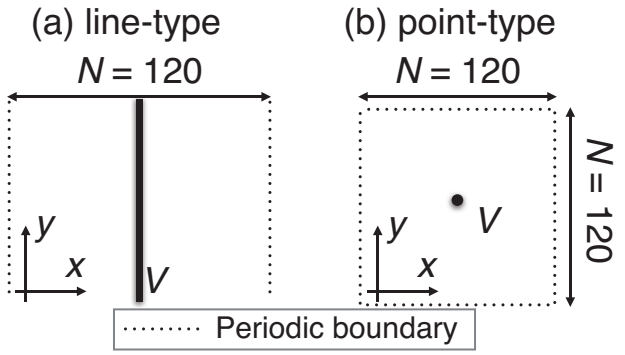

Fig. 1. Schematic diagrams of a system with (a) line-type potential and (b) point-type potential.

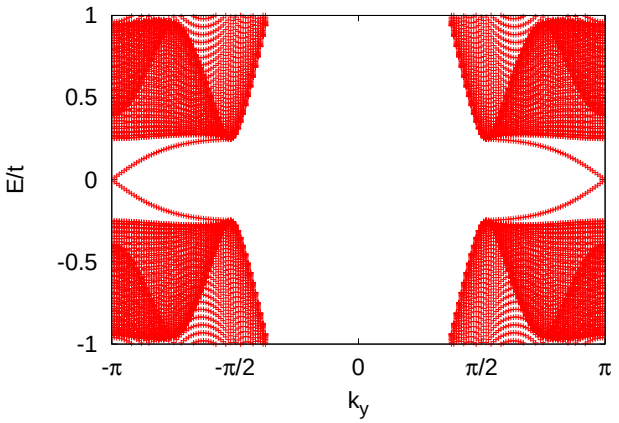

Fig. 2. (Color online) Quasiparticle spectrum for a ultra-high line-type potential function ($V = 100t$), along y-axis. See Fig. 1(a), as well. The pair potential is $\Delta = 0.35t$, and the chemical potential is $\mu = 3.5t$. Since we set the Zeeman magnetic field as $h = 1t$, the system without the potential stays at a topological phase [See, Eq. (6]. The gapless states appear at $k_y = \pm\pi$.

spectrum of the system. Therefore, these MGSs can continuously connect with the zero-energy states, when V increases. Another evidence for the MGSs to be related to the zero-energy states is obtained, calculating the local density of states (LDOS). Figure 4 shows the local density of states at energy $E = 7.4559 \times 10^{-2}\,t$, for $V = 5\,t$. This energy corresponds to the lowest absolute eigenvalue of the Hamiltonian. We find that the corresponding states are located on the surfaces of the potential wall. The spin-imbalanced behavior in the LDOS attributes to the Zeeman magnetic field and the chemical-potential value; the first and the second terms in Eq. (4) imply that the down-spin component mainly contributes to the LDOS near zero energy.

Now, we turn into a systematic study of the quasiparticle spectrum under the line-type potential, varying h and V. Figure 5(a) shows a h-V diagram of the lowest absolute eigenvalue. Figure 5(b) shows a section of the h-V diagram, with $h = 1\,t$. The critical magnetic field for the topological transi-

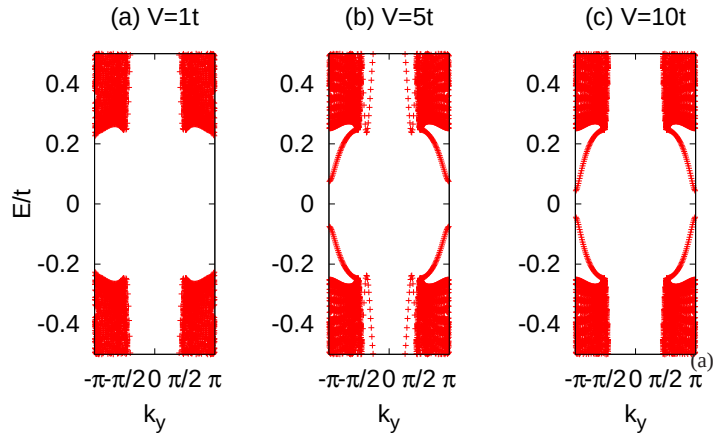

Fig. 3. (Color online) Quasiparticle spectrum for line-type potential, with different barrier heights. The other physical parameters are the same as in Fig. 2. When $V \geq 5t$, the mid-gap states appear.

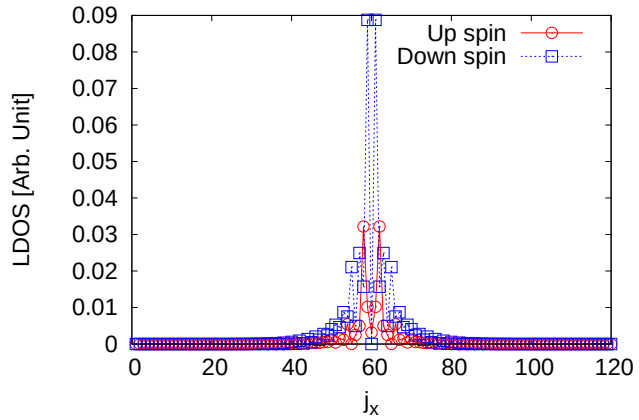

Fig. 4. (Color online) Spin-resolved local density of states, at energy $E = 7.4559 \times 10^{-2} t$, for line-type potential with height $V = 5t$. See Fig. 3(b), as well. The other parameters are the same as in Fig. 2.

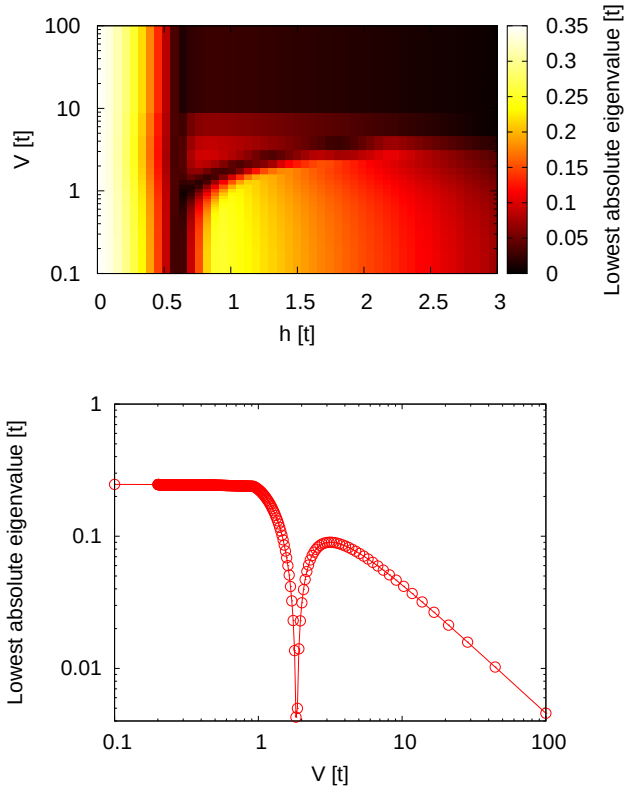

Fig. 5. (Color online) (a) Eigenvalue of tight-binding Hamiltonian (1), with the lowest absolute value, for line-type potential. The magnetic field h (the horizontal axis) and the potential height V (the vertical axis, with logarithmic scale) are changed. We set the pair potential $\Delta = 0.35t$ and the chemical potential $\mu = 3.5t$. The black color means the existence of the zero-energy states. (b) Section in (a), with a fixed magnetic field strength ($h = 1t$). The value at $V = 0.1t$ corresponds to the bulk spectral gap. Therefore, the behavior for $V > 2t$ indicates the presence of the mid-gap states.

tion is $h \approx 0.61\,t$, from Eq. (6). We focus on the case when $h > 0.61\,t$ (i.e., topological phase). For a high-barrier region ($V > 5\,t$), we find the appearance of the MGSs, which is indicated by the dark-colored area in Fig. 5(a). Figure 5(b) shows that the energy of the MGSs is proportional to $1/V$. For a ultra-low barrier region ($V < 1\,t$), the lowest absolute eigenvalue does not significantly reduce. Indeed, we can find that this quantity is equal to the lowest energy of the bulk states. Therefore, no MGS is excited by the ultra-low potential. We obtain a curious result when $1\,t < V < 5\,t$. The lowest absolute eigenvalue is zero (i.e. gap closing) at the specific potential height, depending on h. Figure 5(b) also shows this behavior manifestly. We show an interpretation for this anomalous gap-closing behavior in Sec. 4.1.

4.2 Point-type potential

The results in the previous subsection show that the potential is regarded as a rigid wall when $V = 100\,t$. Our next concern is to examine whether the same behavior occurs in different settings. We examine the point-type potential, as a line setting with ultimately-short line length. We mainly show the characters of the lowest absolute eigenvalue of the Hamiltonian to examine the presence of zero-energy bound states.

Let us study point-type potential (3), as seen in Fig. 2(b). We set $N_x = N_y = 120$, with the periodic boundary condition. Our calculations focus on the case for $h > 0.61\,t$ (topological phase). Figure 6 shows the spin-resolved LDOS at energy $E = 9.8290 \times 10^{-2}\,t$, with $h = 2\,t$ and $V = 100\,t$. This energy is the lowest absolute eigenvalue of the Hamiltonian. We find that the bound states occur around the point potential, with non-zero energy. Figure 7 shows the h-dependence of the lowest absolute eigenvalue of the Hamiltonian, with different heights $V = 5\,t$ and $100\,t$. The curve for $V = 0$ is calculated by exact bulk energy spectrum (5). This curve predominates the plots for $V \neq 0$. The behavior for large V (e.g.,$V = 100\,t$) is consistent with the calculations of the MGSs in a similar

model to the present one by Hu *et al.*[25] The point-type potential leads to the MGSs at the potential center. However, the zero-energy bound states are not induced by the potential. (See, Table I). We are going to argue this point in Sec.5.2.

Now, we study the relation of the mid-gap-state appearance to the decrease of T_c in the 2D topological *s*-wave superconductor. Since the point-type potential is regarded as the scattering center of a single non-magnetic impurity, the point setting is relevant to the previous T-matrix calculations.

Let us focus on the results in the ultra-high potential barrier (blue squares) shown in Fig. 7. We denote the lowest absolute eigenvalue as $E_V^{\rm LA}$. $E_{V=0}^{\rm LA}$ corresponds to the spectrum gap in the DOS without impurities (the green dashed line in Fig. 7). Moreover, we denote the ratio of $E_V^{\rm LA}$ to $E_{V=0}^{\rm LA}$ as $\epsilon_V^{\rm LA}$ $(= E_V^{\rm LA}/E_{V=0}^{\rm LA})$; $\epsilon_V^{\rm LA}$ is the lowest quasiparticle energy normalized by the spectrum gap in the clean limit. The data in Fig. 7 indicates that $\epsilon_{V=100\,t}^{\rm LA}$ decreases when h increases. We can find that $\epsilon_{V=100t}^{\rm LA} \approx 0.72$ for $h = 1\,t$, $\epsilon_{V=100t}^{\rm LA} \approx 0.66$ for $h = 2\,t$, and $\epsilon_{V=100t}^{\rm LA} \approx 0.6$ for $h = 3\,t$. Thus, for a relatively high magnetic field, the quasiparticles with mid-gap energy are much easily excited by impurities. These behaviors are consistent with our previous calculations.[27] The decrease of T_c is not significant for $h = 1t$ [Fig.5(a) in Ref.27], while is pronounced for $h = 2t$ [Fig.5(b) in Ref.27]. Therefore, the location of the MGSs in energy domain can lead to understanding how the robustness of the present model against impurities is ruled by the magnetic field. Systematic studies, such as dependence on scattering models and full self-consistent calculations are needed for the precise location of the poles leading to a significant decrease of T_c by a non-magnetic impurity.

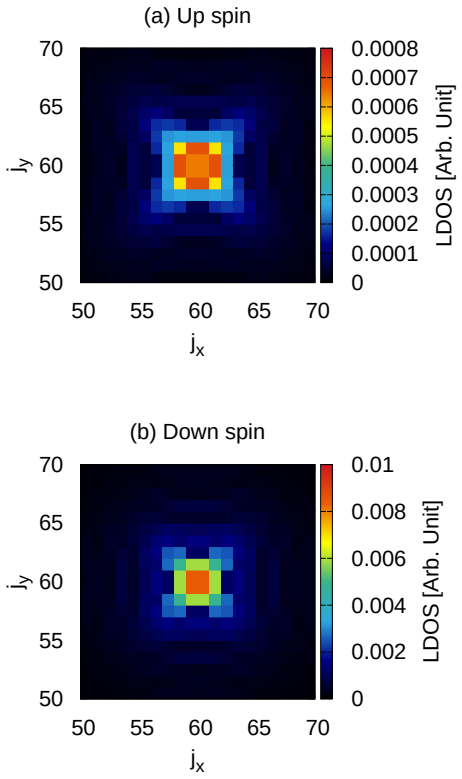

Fig. 6. (Color online) Spin-resolved local density of states at energy $E = 9.8290 \times 10^{-2}t$ in the system with a point-type potential ($V = 100t$). See, Fig. 1(b). The Zeeman magnetic field is $h = 2t$. The other parameters are the same as in Fig. 2. (a) Up spin component and (b) down spin component of the wave functions. We note that in this figure we focus on the area around the potential center.

5. Discussions

5.1 h-V diagram for line-type potential

Let us explain the behaviors on the *h*-*V* diagram shown in Fig. 5, in terms of a topological number, The topological number for classifying the present 2D topological superconductor is the TKNN number.[26] The bulk topological superconducting state for $(3\,t >) h > 0.6\,t$ and $\mu > 2\,t$ has the topological number $N = 1$, as seen in Ref. 15. Since the potential height is moderate, we may consider a local property of the topological state *on* the line (effective 1D superconducting system). The effective chemical potential on the line can be $\mu - V$, owing to the local filling change via the potential. According to the typical arguments in a 1D Majorana nanowire in a semiconductor-superconductor-junction device (e.g. Ref. 20), we may write a "local" topological number on the line as M, although the rigorous treatment requires a infinitely-extended spatial geometry (momentum preservation). We calculate M by the TKNN number in the system with chemical potential $\mu - V$, simply dropping the effects of the boundaries between the potential region and the others. In other words, the number M is the TKNN number for the case when the potential width extends into the whole of the system. Although a one-dimensional class D superconductor is characterized by $\mathbb{Z}_2$,[33] we use the TKNN number (i.e., $\mathbb{Z}$) in this paper since our aim is to compare the "line-shaped" area with the other area (e.g., the area on the left of the line potential) using the common index. Repeating a similar argument to the derivation of Eq. (6), we find that this number takes a non-zero value (i.e., $M = 1$) when

$$h > \sqrt{[4t - (\mu - V)]^2 + \Delta^2}. \tag{7}$$

Let us divide the *h*-*V* diagram into three regions, using Eqs. (6) and (7), as shown in Fig. 8. The red solid line is defined by Eq. (6), whereas the blue dashed one is by Eq. (7). We find that the latter line qualitatively reproduces the line of the zero-energy bound states in Fig. 5(a).

Now, let us summarize phase diagram, as seen in Fig. 8(a). In phase I, the absence of the MGSs is found, since the system is topologically trivial ($N = M = 0$). On the boundary between phases I and III, the energy gap in bulk spectrum (5) closes. In phase II, there is no MGS. This comes from the fact that the topological number N is the same as M (i.e., $N = M = 1$). On the boundary between phases II and III, the energy gap of the "bulk" spectrum in the effective 1D system closes. In phase III, the appearance of the MGSs is found in the vicinity of the potential wall, since the topological number N is different from M (i.e., $N = 1$ and $M = 0$). Taking the ultra-high potential limit in phase III leads to the occurrence

Table I. Difference between line-type and point-type potentials. Anomalous gap-closing is discussed in Sec. 4.1.

	Line-type potential	Point-type potential
Bound states ($V \to \infty$)	Zero energy	Non-zero energy
Anomalous gap-closing	Yes	No

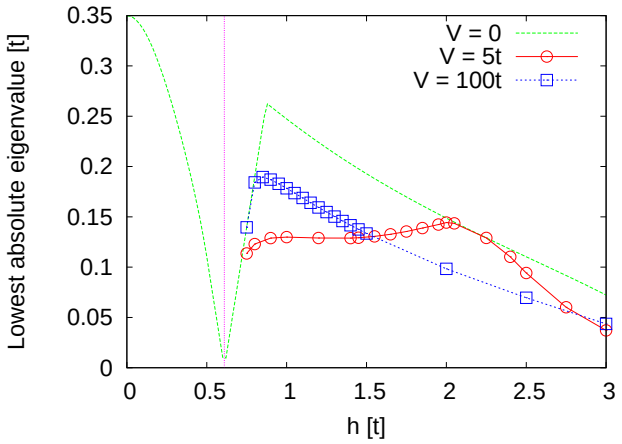

Fig. 7. (Color online) Magnetic-field dependence of the lowest absolute eigenvalue for point-type potential, with heights $V = 5t$ and $V = 100t$. The dashed line ($V = 0t$) is obtained by exact bulk energy spectrum (6). The other parameters are the same as in Fig. 2.

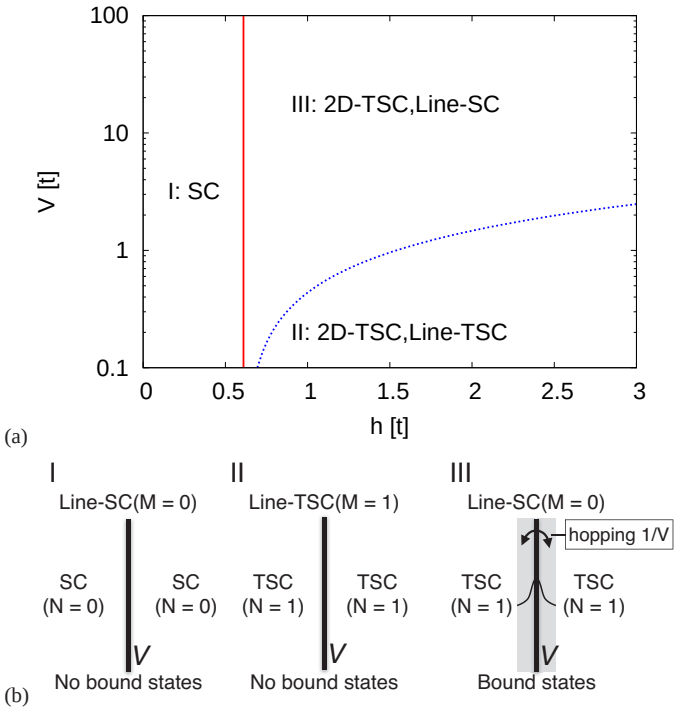

Fig. 8. (Color online) (a) Phase diagram with respect to a topological invariant. The red solid line denotes the topological phase transition in the bulk, defined by Eq. (6). The blue dotted line denotes the topological phase transition on the line-potential, defined by Eq. (7). (b) Schematic diagram of the different phases. The phase III only has the bound states at the boundary.

of the two zero-energy bound states, one of which is located on the left side of the potential barrier, and the other of which is on the right side. Reducing the potential height leads to the hybridization of these two zero-energy states, with hopping proportional to $1/V$; as a result, the degenerate zero eigenvalue is split. These arguments are sketched in Fig. 8(b).

We remark that there is the difference between the numerical calculation [Fig. 5(a)] and the diagram in Fig. 7(a). This difference comes from the fact that the latter diagram is obtained by the TKNN number in the two-dimensional system, not a genuine topological number in a one-dimensional (line) system. It is an interesting future issue to characterize our numerical results via a more definite topological number in a line system.

5.2 Non-zero-energy bound states in point-type potential

The absence of the zero-energy bound states is curious in the point-type potential with ultra-high barrier ($V = 100\,t$). Hu *et al.*[25] discussed a link of non-zero bound states around a non-magnetic impurity with the gapless surface modes, using a finite-confinement effect in the chiral p-wave superfluid surrounded by a disk-shaped rigid wall. Their arguments are interesting, but the map of the present model to a chiral p-wave model is attainable when $h \to \infty$ (We will show the derivation of the map in Sec.5.3). Therefore, other ideas are desirable for explaining the difference from zero energy and a link to the gapless surface modes in a finite magnetic field.

Let us consider this issue, from the viewpoint of continuous deformation of the potential shape from a line to a point. We find the presence of the gapless surface modes in the line-type potential with $V = 100\,t$; the system is separated by the line defect. Figure 4 shows that the bound states accommodate in the both sides of the potential region. When one shortens the line length, the separated regions are connected with each other. Then, interference would occur between the left and the right zero-energy bound states. Thus, we speculate that the zero-energy bound states in the line defect would acquire non-zero energy in a point setting owing to the lack of spatial separation. We will examine the validity of this idea in future.

5.3 Mixture of chiral p-wave and s-wave components

Let us derive an effective theory to understand the numerical results. Our approach is similar to a low-energy theory in the semiconductor-superconductor junction systems,[20] but we take a high-order correction to our description.

We focus on the spatial uniform case. We seek the low-energy region for constructing the effective theory, via the examination of the normal-part BdG Hamiltonian [Eq. (4), with $\Delta = 0$]. The energy eigenvalues in the particle sub-

space ($\tau^3 = 1$) are $E^{\pm}_{\mathrm{n},\boldsymbol{k}} = \varepsilon_{\boldsymbol{k}} \pm \sqrt{h^2 + \alpha^2|\boldsymbol{\ell}_{\boldsymbol{k}}|^2}$. We focus on the case when the chemical potential is located at the intermediate energy between the higher band and the lower band. All the previous calculations in this article correspond to this case. Hence, the Fermi surface is determined by the solution of $0 = E^{-}_{\mathrm{n},\boldsymbol{k}}$. Since $E^{+}_{\mathrm{n},\boldsymbol{k}} - E^{-}_{\mathrm{n},\boldsymbol{k}} \geq 2h$, the higher-energy contributions are negligible, when $h \to \infty$. A high magnetic-field value indicates that the electron spin is almost polarized upward. Thus, the low-energy subspace is attainable by the spin-up projector $(1/2)(s^0 + s^3) \otimes \tau^0$.

The effective theory is built up by a perturbation approach, in the vicinity of the Fermi surface. The order of the perturbative expansions is evaluated by α/h since the spin-orbit coupling mixes the low-energy sector (spin up) with the high-energy sector (spin down). Also, the ratio of $|\Delta|$ to h should be small since the perturbation term contains the contributions of the pairing potential. Thus, the expansions are valid when $h \gg \alpha$, $|\Delta|$. Before the perturbative expansions, we perform a basis transformation to take a higher-order correction. The procedure is similar to the Tani-Foldy-Wouthuysen transformation[30] for the Dirac equation. The unitary-transformed BdG Hamiltonian is $\mathcal{H}_{\boldsymbol{k},\eta} = \mathcal{S}_\eta \mathcal{H}_{\boldsymbol{k}} \mathcal{S}_\eta^{-1}$, with

$$\mathcal{S}_\eta = \exp\left[i\frac{\eta}{2} s^3 \otimes \left(\frac{i\Delta}{|\Delta|}\tau^+ + \mathrm{h.c.} \right) \right]. \tag{8}$$

We take so small angle η that $\eta \sim O(\alpha/h)$. In other words, we partially diagonalize the Hamiltonian, with the restricted rotation $\mathcal{S}$. We choose a free part of $\mathcal{H}_{\boldsymbol{k},\eta}$, as seen in Eq. (A·1) in Appendix . Then, the 2nd-order Brillouin-Wigner approach[31] leads to an effective Hamiltonian,

$$\begin{aligned} \mathcal{H}^{\mathrm{eff}}_{\boldsymbol{k}} &= \frac{s^0 + s^3}{2} \otimes \left[\frac{\tau^0 + \tau^3}{2} h^{\mathrm{eff}}_{\boldsymbol{k}} + \frac{\tau^0 - \tau^3}{2} (-h^{\mathrm{eff}}_{-\boldsymbol{k}})^* \right. \\ &\quad \left. + (i\Delta^{\mathrm{eff}}_{\boldsymbol{k}}\tau^+ + \mathrm{h.c.}) + O(\alpha^2/h^2) \right], \end{aligned} \tag{9}$$

with $h^{\mathrm{eff}}_{\boldsymbol{k}} = \varepsilon_{\boldsymbol{k}} - h - (\alpha^2/h)|\boldsymbol{\ell}_{\boldsymbol{k}}|^2 + (|\Delta|^2/h)$ and

$$\Delta^{\mathrm{eff}}_{\boldsymbol{k}} = -\frac{2\alpha}{h}\Delta(\ell_{2,\boldsymbol{k}} + i\ell_{1,\boldsymbol{k}}) - \frac{2i\eta|\Delta|}{h}\Delta. \tag{10}$$

The detail calculations are shown in Appendix , but we concisely illustrate how effective gap function (10) is produced from the original s-wave mean-filed term. In Eq. (4), the spin-orbit couplings (the second line) do not commute with the pairing potential term (the third line). Thus, in the perturbation analysis, the cross terms between them may exist, and they lead to the effective superconducting gaps. When $\eta \to 0$ (i.e., no unitary transformation is performed), the chiral p-wave low-energy behavior is survived, whereas the s-wave contribution disappears. This result is consistent with the low-energy theory in the semiconductor-superconductor junction systems.[20] Therefore, the full gap feature emerges as a higher-order correction in the low-energy effective Hamiltonian. When a magnetic field is high, the chiral p-wave component is predominant.

A similar argument is possible for a 3D topological superconductor. The low-energy effective theory is attainable, taking large-mass (nonrelativistic) limit.[34] This assertion is reasonable, since the Zeeman magnetic field in the 2D topological superconductor is regarded as the mass term. Moreover, we mention that, taking massless (ultrarelativistic) limit[34,35] (i.e. a weak magnetic field in our system), the superconductivity is robust against non-magnetic impurities, like s-wave superconductivity.

The mixture of the chiral p-wave and s-wave characters in the effective gap is interesting. It indicates that the robustness of the present model against non-magnetic impurities can differ from typical behaviors in a chiral p-wave model when the s-wave correction is negligible. We find that in the point setting (Sec. 4.2) the system is relatively robust around $h = 1\,t$. Since we set $\alpha = 1\,t$ throughout this article, this robustness can be related to the s-wave correction. It is an intriguing task to compare the present model with a chiral p-wave model. The chiral p-wave superconductors also lead to the bound states with almost zero energy around a non-magnetic impurity.[36] One can expect that the 2D topological s-wave superconductor has a lot of behaviors similar to the ones in the chiral p-wave superconductor. However, we guess that the quantitative differences are not negligible in an intermediate magnetic field (e.g., $h \gtrsim \alpha$) since the map to chiral p-wave is attainable by perturbation with $h \gg \alpha$. Clarifying the difference from a chiral p-wave model in the impurity effects is an important future issue.

6. Summary

We studied how the MGSs appear in the 2D topological s-wave superconductors with spatial inhomogeneity. Two kinds of the potential functions, line-type potential and point-type one were examined. The line setting showed a definite link between the MGSs and the gapless surface modes. The point setting showed that the quasiparticles with mid-gap energy are much easily excited by impurities when the Zeeman magnetic field increases. This result supports our previous calculations[27] of the decrease of T_{c} by non-magnetic impurities. To understand the numerical results, we derived an effective theory applicable to high magnetic fields. The effective gap was the mixture of the chiral p-wave and s-wave components. The former is predominant when the magnetic field increases. Therefore, we claim that a chiral p-wave feature in the effective gap function creates the MGSs.

Acknowledgements

We thank H. Nakamura, A. Shitade and K. Kobayashi for helpful discussions and comments. The calculations were performed using the supercomputing system PRIMERGY BX900 at the Japan Atomic Energy Agency. This study has been partially supported by JSPS KAKENHI Grant Number 24340079, 26800197.

Appendix: Derivation of an effective Hamiltonian

We show the derivation of Eq. (9). We start with the unitary-transformed BdG Hamiltonian $\mathcal{H}_{\boldsymbol{k},\eta} = \mathcal{S}_\eta \mathcal{H}_{\boldsymbol{k}} \mathcal{S}_\eta^{-1}$, where $\mathcal{S}_\eta$ is defined by Eq. (8). We take so small angle η that $\eta \sim O(\alpha/h)$. After straightforward calculations, we find that

$\mathcal{H}_{\boldsymbol{k},\eta} = \mathcal{H}^{(0)}_{\boldsymbol{k},\eta} + \mathcal{V}_{\boldsymbol{k},\eta} + O(\eta^2)$, with

$$\begin{aligned}\mathcal{H}^{(0)}_{\boldsymbol{k},\eta} &= \frac{s^0+s^3}{2}\otimes[(\varepsilon_{\boldsymbol{k}}-h)\tau^3 + (i\Delta^{(+)}_{\boldsymbol{k},\eta}\tau^+ + \text{h.c.})] \\ &\quad + \frac{s^0-s^3}{2}\otimes[(\varepsilon_{\boldsymbol{k}}+h)\tau^3 + (i\Delta^{(-)}_{\boldsymbol{k},\eta}\tau^+ + \text{h.c.})],\end{aligned} \tag{A·1}$$

$$\begin{aligned}\mathcal{V}_{\boldsymbol{k},\eta} &= s^1\otimes(\alpha\ell_{1,\boldsymbol{k}} + i\Delta^{(1)}_{\eta})\tau^0 \\ &\quad + s^2\otimes[\alpha\ell_{2,\boldsymbol{k}}\tau^3 + (i\Delta^{(2)}_{\boldsymbol{k},\eta}\tau^+ + \text{h.c.})].\end{aligned} \tag{A·2}$$

The four additional gap functions are $\Delta^{(\pm)}_{\boldsymbol{k},\eta} = \mp i\eta(\varepsilon_{\boldsymbol{k}} \mp h)(\Delta/|\Delta|)$, $\Delta^{(1)}_{\eta} = -i\eta|\Delta|$, and $\Delta^{(2)}_{\boldsymbol{k},\eta} = [1-(\eta\alpha\ell_{1,\boldsymbol{k}}/|\Delta|)]\Delta$. We set the free part for the perturbation approach as $\mathcal{H}^{(0)}_{\boldsymbol{k},\eta}$.

Now, we derive the low-energy effective Hamiltonian. The 2nd-order Brillouin-Wigner approach[31] leads to an effective Hamiltonian

$$\mathcal{H}^{\text{eff}}_{\boldsymbol{k}} = \mathcal{P}\mathcal{H}^{(0)}_{\boldsymbol{k},\eta}\mathcal{P} + \sum_{m=1}^{2}(\mathcal{P}\mathcal{V}_{\boldsymbol{k},\eta}\mathcal{Q})\mathcal{R}_{\boldsymbol{k},\eta,m}(\mathcal{Q}\mathcal{V}_{\boldsymbol{k},\eta}\mathcal{P}), \tag{A·3}$$

with $\mathcal{P} = (1/2)(s^0+s^3)\otimes\tau^0$, $\mathcal{Q} = s^0\otimes\tau^0 - \mathcal{P}$ and $\mathcal{R}_{\boldsymbol{k},\eta,m} = \mathcal{Q}[E^{(0)}_{\boldsymbol{k},\eta,m} - \mathcal{Q}\mathcal{H}^{(0)}_{\boldsymbol{k},\eta}\mathcal{Q}]^{-1}$. The non-perturbative energy $E^{(0)}_{\boldsymbol{k},m}$ is related to the eigenvalues of $\mathcal{P}\mathcal{H}^{(0)}_{\boldsymbol{k},\eta}\mathcal{P}$: $\mathcal{P}\mathcal{H}^{(0)}_{\boldsymbol{k},\eta}\mathcal{P} = (1/2)(s^0+s^3)\otimes\text{diag}\{E^{(0)}_{\boldsymbol{k},\eta,1}, E^{(0)}_{\boldsymbol{k},\eta,2}\}$. We approximate $\mathcal{R}_{\boldsymbol{k},\eta,m}$ by the value on the Fermi surface, $\mathcal{R}_{\boldsymbol{k},\eta,m} \approx \mathcal{R}_{\boldsymbol{k}_{\text{F}},\eta,m}$, with the Fermi momentum $\boldsymbol{k}_{\text{F}}$ given by $\epsilon_{\boldsymbol{k}_{\text{F}}} = h + O(\alpha^2/h^2)$. Taking the leading term,[32] we find that $R_{\boldsymbol{k},\eta,m} \approx (1/2)(s^0-s^3)\otimes(-1/2h)\tau^3$. Therefore, performing straightforward algebraic calculations about the Pauli matrices, we obtain Eq. (9). In the effective gap $\Delta^{\text{eff}}_{\boldsymbol{k}}$, the chiral p-wave component (the first term) comes from $\Delta^{(2)}_{\boldsymbol{k},\eta}$. In contrast, the s-wave component (the second term) is attributable to $\Delta^{(1)}_{\eta,\boldsymbol{k}}$. We remark that the contribution from $\Delta^{(+)}_{\boldsymbol{k},\eta}$ in Eq. (A·1) is negligible, since on the Fermi surface $\Delta^{(+)}_{\boldsymbol{k},\eta} \sim \eta O(\alpha^2/h^2) \sim O(\alpha^3/h^3)$. The contribution from $\Delta^{(-)}_{\boldsymbol{k},\eta}$ is irrelevant to the low-energy sector, owing to the spin-up projector $\mathcal{P}$.

1) P. W. Anderson, J. Phys. Chem. Solids, **11**, 26 (1959).
2) T. Tsuneto, Prog. Theore. Phys. **28**, 857 (1962).
3) P. G. de Gennes, *Superconductivity of Metals and Alloys* (Westview Press, Boulder, 1999) Chap.8.
4) N. B. Kopnin, *Theory of Nonequilibrium Superconductivity* (Oxford University Press, New York, 2001).
5) A. V. Balatsky, I. Vekhter, and J.-X. Zhu, Rev. Mod. Phys. **78**, 373 (2006).
6) P. Hirschfeld, D. Vollhardt, and P. Wölfle, Solid State Commun **59**, 111 (1986).
7) S. Schmitt–Rink, K. Miyake, and C. M. Varma, Phys. Rev. Lett. **57**, 2575 (1986).
8) T. Hotta, J. Phys. Soc. Jpn. **62**, 274 (1993).
9) G. Preosti and P. Muzikar, Phys. Rev. B **54**, 3489 (1996).
10) K. Maki and E. Puchkaryov, Europhys. Lett. **45**, 263 (1999).
11) K. Maki and E. Puchkaryov, Europhys. Lett. **50**, 533 (2000).
12) L. Fu and E. Berg, Phys. Rev. Lett. **105**, 097001 (2010).
13) M. Sato, Phys. Rev. B **81**, 220504(R) (2010).
14) M. Sato, Y. Takahashi, and S. Fujimoto, Phys. Rev. Lett. **103**, 020401 (2009).
15) M. Sato, Y. Takahashi, and S. Fujimoto, Phys. Rev. B **82**, 134521 (2010).
16) E. Fradkin, *Field Theories of Condensed Matter Physics* (Cambridge University Press, Cambridge, UK, 2013) Chap.15.
17) N. Read and D. Green, Phys. Rev. B **61**, 10267 (2000).
18) J. C. Y. Teo and C. L. Kane, Phys. Rev. B **82**, 115120 (2010).
19) Y. Nishida, Phys. Rev. D **81** 074004 (2010).
20) J. Alicea, Y. Oreg, G. Refael, F. von Oppen, and M. P. A. Fisher, Nat. Phys. **7**, 412 (2011).
21) Y. Ohashi, Phys. Rev. A **83**, 063611 (2011).
22) J. D. Sau and E. Demler, Phys. Rev. B **88**, 205402 (2013).
23) M. Ichioka and K. Machida, Phys. Rev. B **76**, 064502 (2007).
24) K. V. Samokhin, in *Non-Centrosymmetric Superconductors: Introduction and Overview*, ed. E. Bauer and M. Sigrist (Springer, Heidelberg, 2012) p.269.
25) H. Hu, L. Jiang, H. Pu, Y. Chen, and X.-J. Liu, Phys. Rev. Lett. **110**, 020401 (2013).
26) D. J. Thouless, M. Kohmoto, M. P. Nightingale, and M. den Nijs, Phys. Rev. Lett. **49**, 405 (1982).
27) Y. Nagai, Y. Ota, and M. Machida, J. Phys. Soc. Jpn., **83**, 094722 (2014).
28) T. Sakurai and H. Sugiura, J. Comput. Appl. Math. **159**, 119 (2003).
29) Y. Nagai, Y. Shinohara, Y. Futamura, Y. Ota, and T. Sakurai, J. Phys. Soc. Jpn. **82**, 094701 (2013).
30) C. Itzykson and J.-B. Zuber, *Quantum Field Theory* (Dover, New York, 2005).
31) I. Hubač and S. Wilson, *Brillouin-Wigner Methods for Many-Body Systems* (Springer, Heidelberg, 2010).
32) A definite formula is $\mathcal{R}_{\boldsymbol{k}_{\text{F}},\eta,m} = (1/2)(s^0-s^3)\otimes[(-1/2h)\tau^3 + (-\eta/2h|\Delta|)(i\Delta\tau^+ + \text{h.c.}) + O(\eta^2)]$. The correction from the second term in the above formula to Eq. (9) is an overall (non-zero) complex-number constant in the s-wave contribution.
33) A. P. Schnyder, S. Ryu, A. Furusaki, and A. W. W. Ludwig, Phys. Rev. B **78**, 195125 (2008).
34) Y. Nagai, Y. Ota, and M. Machida, Phys. Rev. B **89**, 214506 (2014).
35) K. Michaeli and L. Fu, Phys. Rev. Lett. **109**, 187003 (2012).
36) M. Takigawa, M. Ichioka, K. Kuroki, and Y. Tanaka, Phys. Rev. B **72**, 224501 (2005).